Journal of Nano- and Electronic Physics
Vol. **12** No 3, 03003(5pp) (2020)

Журнал нано- та електронної фізики
Том **12** № 3, 03003(5cc) (2020)

Enhancement of Performance of *a*-Si:H Solar Cells by Introducing a *p-nc*-SiO*x*:H Nanostructure Buffer Layer

A. Belfar[1,*], A.J. Garcia-Loureiro[2]

[1] *Laboratory of Plasma Physics, Conductor Materials and their Applications, Faculty of Physics, Oran University of Sciences and Technology Mohamed Boudiaf USTO-MB, BP1505 Oran, Algeria*
[2] *Centro de Investigación en Tecnoloxías da Información (CITIUS), University of Santiago de Compostela, Santiago de Compostela, Spain*

(Received 14 January 2020; revised manuscript received 15 June 2020; published online 25 June 2020)

In this work, single *n-i-p* solar cells based on hydrogenated amorphous silicon (*a*-Si:H) are analyzed using one dimensional AMPS-1D (Analysis of Microelectronic and Photonic Structures) code. Effect of introducing a *p*-layer based on hydrogenated nanocrystalline silicon oxide (*p-nc*-SiO$_x$:H) as a buffer layer at *i/p* interface instead of *i*-layer based on hydrogenated amorphous silicon carbide (*i-a*-SiC:H) is analyzed. It is found that the incorporation of *p-nc*-SiO$_x$:H buffer layer at *i/p* interface reduces the band mismatch between *i-a*-Si:H absorber layer and p^+-*nc*-SiO$_x$:H window layer and minimizes the defect density near interface. It is also obtained that the spectral response of the solar cell has improved in the wavelength range from 0.48 to 0.7 μm with using *p-nc*-SiO$_x$:H window/*p-nc*-SiO$_x$:H buffer dual *p*-layers. So, an enhancement of the output solar cell performances with using *p-nc*-SiO$_x$:H buffer layer has obtained. In this case, the short circuit current (J_{sc}) increases from 10.18 mA/cm^2 with *i-a*-SiC:H buffer layer to 13.44 mA/cm^2 with *p-nc*-SiO$_x$:H buffer layer, the open circuit voltage (V_{OC}) improves from 930 mV to 941 mV and the fill factor (FF) increases from 74.2 % to 76.5 %. As a consequence, the conversion efficiency increases from 7.03 % to 9.67 %.

Keywords: Solar cell, *a*-Si:H, *p-nc*-SiO$_x$:H, *i-a*-SiC:H, Buffer layer, Simulation, Spectral response.

DOI: 10.21272/jnep.12(3).03003 PACS numbers: 73.40.Lq, 78.20.Bh

1. INTRODUCTION

It is known that the *i/p* interface is a heterojunction with band mismatch between energy bands of an intrinsic absorber layer and a wide band-gap of a *p*-window layer. In the case of devices based on hydrogenated amorphous silicon (*a*-Si:H), the solar cell performances depend on the *i/p* interfacial matching [1]. Previous works reported that a large amount of dangling bonds may exist at the *i/p* interface which increases the recombination rate [2-4]. In the past and even nowadays, much attention is paid to the *i/p* interface in order to accommodate the band mismatch and understand the different transport mechanisms that can take place and therefore find the necessary solutions to reduce the recombination rate at this interface. A common solution is to introduce a buffer layer of *a*-SiC:H with graded band gap into the *i/p* interface [5, 6]. View to their best electrical properties and less parasitic optical absorption, the *p-nc*-SiO*x*:H (hydrogenated nanocrystalline silicon oxide) layer is a good candidate to replace the *p-nc*-Si:H and *p-a*-SiO*x*:H for using as a window layer [7, 8]. So, in this work, the numerical simulation allowed us to understand the reasons of the improvement in the *a*-Si:H solar cell output parameters, with *n-i-p* configuration, like short-circuit current (J_{SC}), open circuit voltage (V_{OC}), fill factor (FF) and the conversion efficiency by incorporating a *p*-type buffer layer based on hydrogenated nanocrystalline silicon oxide (*p-nc*-SiO$_x$:H) instead of *i-a*-SiC:H intrinsic buffer layer. For the simulation, the computer code AMPS-1D (One-dimensional Analysis of Microelectronic and Photonic Structures) was used [9].

2. AMPS-1D MODEL FOR AMORPHOUS SILICON AND SIMULATED SOLAR CELLS

The numerical simulation of the photovoltaic structure was carried out using the AMPS-1D software. In this code, three coupled differential equations; the Poisson equation the continuity equations for the electrons and for the holes are solved simultaneously, at equilibrium and out of equilibrium conditions. The simulation was carried out by taking into account the Shockley-Read-Hall (SRH) recombination statistics. For the resolution of the coupled differential equations, AMPS-1D uses the algorithm of Newton Raphson. To simulate the local state density present in the band gap of the materials which constitute the solar cells, it has been assumed the existence of two types of states, the acceptor states and the donor states [9].

3. SIMULATED SOLAR CELLS

For the simulation we considered two solar cells based on hydrogenated amorphous silicon (*a*-Si:H). In the simulated cells and, for the front contact, a transparent conducting oxide (TCO) layer has been deposited on the *p*-side. For the back contact, we have used a metal substrate. The two devices consist of an intrinsic *a*-Si:H active layer with a thickness of 300 nm sandwiched between a 25 nm thick *n-a*-Si:H layer and a 15 nm thick *p-nc*-SiO$_x$:H window layer based on hydrogenated nanocrystalline silicon oxide. In the first cell, an intrinsic buffer layer based on hydrogenated amorphous silicon carbon (*i-a*-SiC:H) has been incorporated between the *p*-window layer and the active layer (Fig. 1a). On the other hand, in the second device the

* abbasbelfar@gmail.com

buffer layer is a *p*-type layer based on hydrogenated nanocrystalline silicon oxide (*p*-*nc*-SiO$_x$:H) (Fig. 1b).

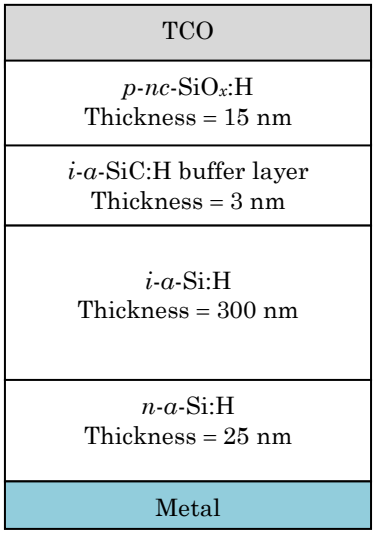

Fig. 1 – Schematic diagram of the simulated solar cells with: *i*-*a*-SiC:H buffer layer (a), *p*-*nc*-SiO$_x$:H buffer layer (b)

4. ELECTRICAL AND OPTICAL INPUT PARAMETERS FOR SIMULATION

Our simulations were performed with the computer code AMPS-1D. The simulation requires two types of electrical and optical input parameters such as surface recombination rates, barrier heights, radiation power density as well as the characteristics of the layers forming the structures. For electron and hole surface recombination velocities, we used the value of 10^7 cm/s. The height of the front Φ_{bo} (TCO/*p*-window layer) and rear Φ_{bL} (*n* layer/metal) contact barriers were set at 1.45 eV and 0.2 eV, respectively. The absorption coefficients for the different layers of each structure are integrated in the AMPS-1D code. The electron affinity (χ) is assumed to be different for the hydrogenated nanocrystalline silicon oxide (*p*-*nc*-SiO$_x$:H) layers and the hydrogenated amorphous silicon (*a*-Si:H) based layers. AM 1.5 solar radiation with a power density of 100 mW/cm^2, as a source of illumination, was adopted. The reflection of light at the front contact (FR) was set at 0.2. For the back contact and since there is no back reflector, we chose 0 for back reflection (BR). All other parameters used in the simulation were obtained in our previous works [2, 10-12].

5. RESULTS AND DISCUSSION

To examine the effect of inserting a buffer layer at the *i*/*p* interface on the external solar cell performances we have simulated two *n*-*i*-*p* solar cells described above. The first cell with *i*-*a*-SiC:H buffer layer and the second with *p*-*nc*-SiO$_x$:H buffer layer. For a thickness of the buffer layer equal to 3 nm, the *J*(*V*) characteristics at direct bias and under illumination are presented in Fig. 2. One can see that the *J*(*V*) curves are sensitive to the type of the incorporated buffer layer at the *i*/*p* interface. However, we can see that there is an amelioration in the output solar cell performances with using *p*-*nc*-SiO*x*:H buffer layer. The short circuit current (*Jsc*) increases from 10.18 mA/cm^3 with *i*-*a*-SiC:H buffer layer to 13.44 mA/cm^2 with *p*-*nc*-SiO*x*:H buffer layer. The open circuit voltage (V_{OC}) changes from 930 mV to 941 mV. The fill factor (FF) improves from 74.2 % to 76.5 %. As a consequence, the efficiency increases from 7.03 % to 9.67 %.

To understand and analyze in depth the reasons of these improvements of the cell external parameters we have calculated and presented at the *i*/*p* interface the energy band diagrams, the electric field, the free holes and the generation rate. The spectral response of the two devices has also been calculated and presented.

Fig. 3 shows the energy band diagram of the two simulated solar cells generated by AMPS-1D. Experimentally, it is verified that during deposition of *i*-*a*-SiC:H buffer layer, the incorporation of carbon atoms by introduction of CH_4 makes the band gap increasing gradually [1, 2]. Notwithstanding, the solar cell performances degraded by using an i-a-SiC:H film which contain disordered structural defects causes by the presence of carbon atoms [14]. However, in the case of *p*-*nc*-SiO$_x$:H window or buffer layer the oxygen is added via the CO_2 flux into the deposited gas mixture. The amount of oxygen in the layer is adjusted by varying the CO_2 flux [15]. In numerical analysis, the oxygen incorporation in the *nc*-Si:H matrix is modeled by higher and different value of E_g for p^+-window layer and *p*-buffer layer. On the one hand, the incorporation of a buffer layer at the *i*/*p* interface helps to lessen the band mismatch between *i*-*a*-Si:H absorber layer and p^+-*nc*-SiO$_x$:H window layer, resulting in the scaling down the defect density near the interface. On the other hand, the recombination rate of carriers is lower in the case of structure with *p*-*nc*-SiO*x*:H buffer layer (Fig. 3a), this is can be attributed to the widened band gap in the conduction band side and, which can also help to prevent the back diffusion of thermal or photo-generated electrons. [1]. The latter idea explains the high density of free holes at the *i*/*p* interface in the case of a structure with *p*-*nc*-SiO$_x$:H buffer layer calculated and presented in Fig. 4. For the device with *i*-*a*-SiC:H buffer layer, a value of $1.42 \cdot 10^{18}$ cm^{-3} is obtained. Insertion of *p*-*nc*-SiO$_x$:H buffer layer decreases the defect density near the interface and increases the

free hole density at *i*/*p* to a value of $6.21 \cdot 10^{18}$ cm^{-3}. The plot of electric field under AM 1.5 illumination, as obtained from the simulation calculations for two different buffer layers at the *i*/*p* interface (Fig. 5), explains the sensitivity of both V_{OC} and FF to the type of buffer layer. If *i*-*a*-SiC:H buffer layer is inserted at the *i*/*p* interface, a large amount of defects are produced due to the presence of carbon atoms. Compared to structure with *p*-*nc*-SiO$_x$:H buffer layer, the high density of captured holes in *i*-*a*-SiC:H buffer layer intensifies the electric field near the p^+-*nc*-SiO$_x$:H window layer/*i*-*a*-SiC:H buffer layer interface, and the electric field is lowered over both *i*-*a*-SiC:H buffer layer and *i*-*a*-Si:H absorber layer.

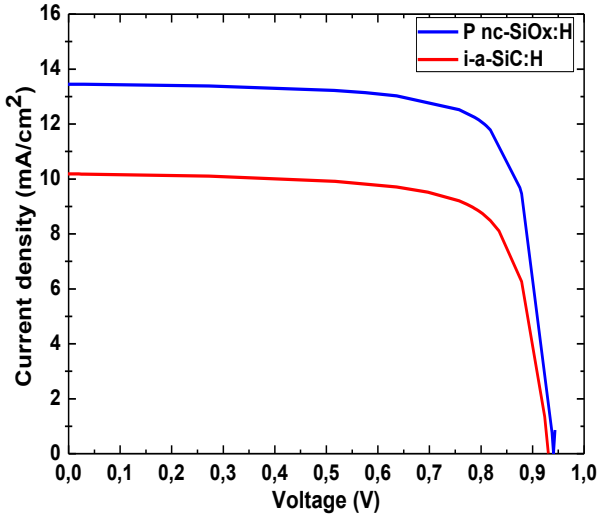

Fig. 2 – The *J*(*V*) curves of simulated solar cells with a thickness of 3 nm for two different buffer layers

The lowered electric field cannot separate efficacy of the photogenerated carriers, which reduces the collections efficiency. All these explain the high values of V_{OC} and FF obtained in the case of a structure with *p*-*nc*-SiO*x*:H buffer layer. This result agrees with the results reported by many groups that the *Voc* is improved by reducing the recombination at the *i*/*p* interface with the introduction of carbide [16, 17], graded boron [18] and

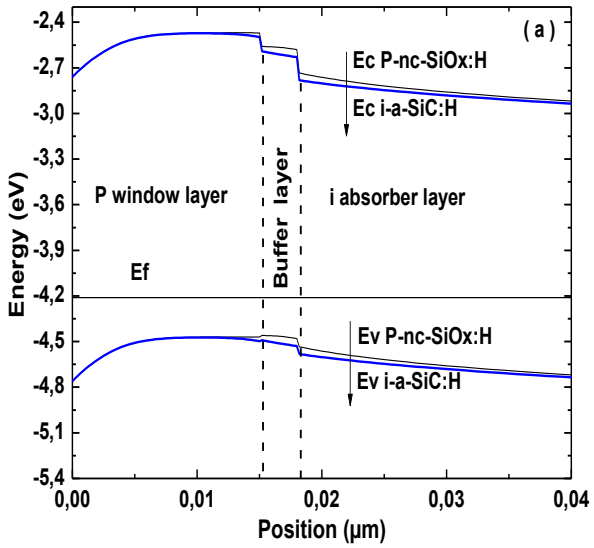

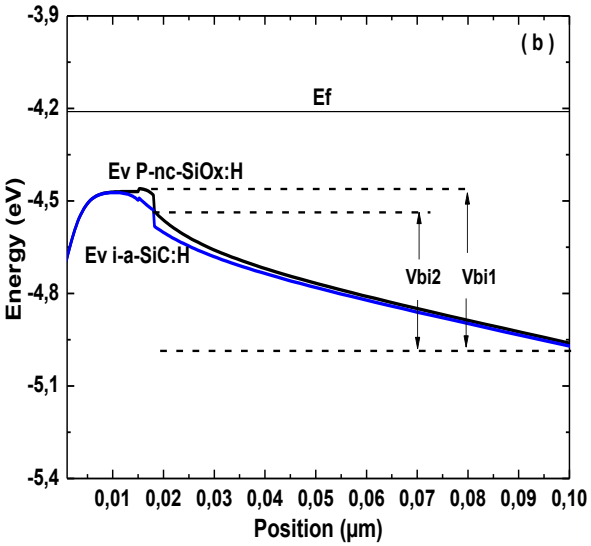

Fig. 3 – Schematic diagram of energy band diagram of *n*-*i*-*p* simulated solar cells with a thickness of 3 nm for two different buffer layers at thermodynamic equilibrium (a) and valence band edge versus position (b)

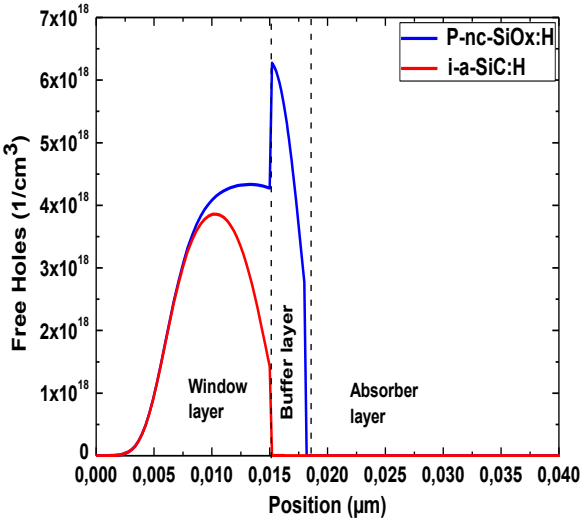

Fig. 4 –Free holes at the *i*/*p* interface for two different buffer layers

graded boron associated with oxygen content buffer layers [19]. Some authors reported that a higher value of the built-in voltage (*Vbi*) improved *Voc* [19].

So, 11 mV slight increase in *Voc* of *a*-Si:H solar cell with *p*-*nc*-SiO$_x$:H buffer layer is due to a high value of V_{bi1} compared to the value of V_{bi2} in the case of a structure with *i*-*a*-SiC:H buffer layer (Fig. 3b). The high value of V_{bi1} probably occurred owing to *p*-*nc*-SiO$_x$:H film with high dark conductivity [19].

It can be seen that the value of J_{SC} (Fig. 2) increases with using *p*-*nc*-SiO$_x$:H buffer layer. However, *Jsc* increases from 10.18 mA/cm^3 with *i*-*a*-SiC:H buffer layer to 13.44 mA/cm^2 with *p*-*nc*-SiO$_x$:H buffer layer. Knowing that, the expression of J_{SC} is given as follows:

$$JSC = q \int_{(\lambda)} \Phi(\lambda)\{1 - R(\lambda)\} QE(\lambda) d\lambda$$

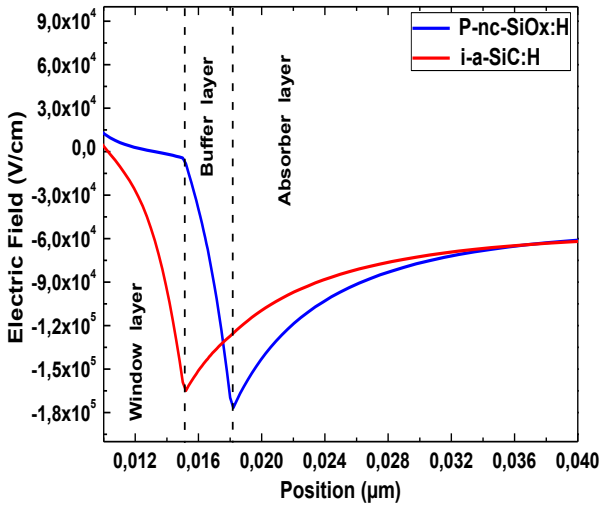

Fig. 5 – Electric field at the *i*/*p* interface for two different buffer layers

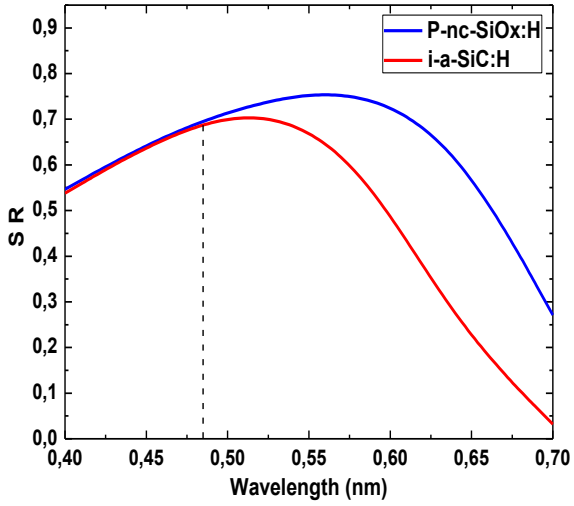

Fig. 6 – Spectral response of the simulated solar cells with a thickness of 3 nm for two different buffer layers

where $QE(\lambda)$ is the quantum efficiency; $R(\lambda)$ is the reflection coefficient from the top surface; $\Phi(\lambda)$ is the photon flux incident on the solar cell at wavelength λ. The integration is carried out over the whole range of wavelengths λ of light absorbed by the structure.

From Fig. 6 we can see that the spectral response of the solar cell has improved in the wavelength range from 0.48 to 0.7 μm in the case of the structure with *p*-*nc*-SiO$_x$:H buffer layer. However, the increment of J_{SC} is obviously due to the improvement of the spectral response (SR). On the one hand, it is known that in order to reduce parasitic absorption and enhance the spectral response of *a*-Si:H solar cell, a wide band gap *p*-type silicon film is used as the window layer [19]. On the other hand, it was clearly shown that to allow more light to be absorbed by the absorber layer in the *a*-Si:H cells it is preferred to us a *p*-*nc*-SiO*x*:H layer which had a lower absorption coefficient than the *p*-*a*-SiO*x*:H layer and than *i*-*a*-SiC:H layer [7, 19]. This can be observed in Fig. 7, when the generation rate is important and reaches a maximum value of $2.4{\cdot}10^{22}$ cm^{-3}s^{-1} at the buffer layer/absorber layer interface in the case of a solar cell with *p*-*nc*-SiO$_x$:H buffer layer compared to the value of $1.2{\cdot}10^{22}$ cm^{-3}s^{-1} for the cell with *i*-*a*-SiC:H buffer layer. Therefore, the dual *p*-layers with *p*-*nc*-SiO$_x$:H window/*p*-*nc*-SiO$_x$:H buffer nanostructure had properties that were superior to those of the dual layers with *p*-*nc*-SiO$_x$:H window/*i*-*a*-SiC:H buffer and became a good option to improve the performances of single *n*-*i*-*p* *a*-Si:H based solar cells.

6. CONCLUSIONS

In this study, we have used AMPS-1D code to examine by numerical simulation the reasons of the improvement of the output parameters (J_{SC}, V_{OC}, FF and Efficiency) of *n*-*i*-*p* *a*-Si:H solar cells when using *p*-*nc*-SiO$_x$:H layer instead of *i*-*a*-SiC:H layer as the buffer layer at the *i*/*p* interface. The simulation results showed that using *p*-*nc*-SiO$_x$:H buffer layer FF can improve by

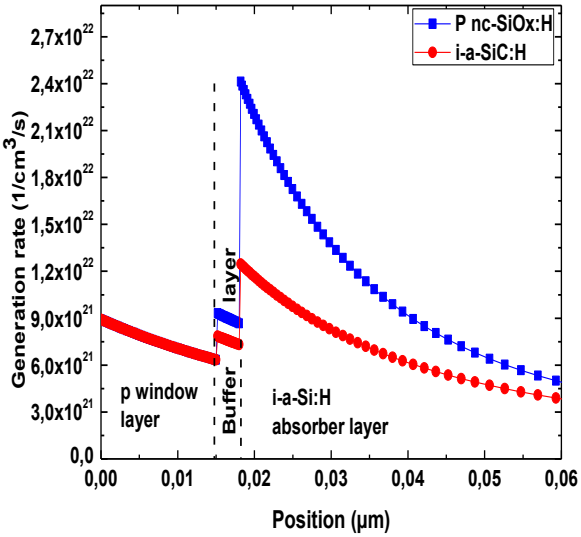

Fig. 7 – Generation rate at the *i*/*p* interface of simulated solar cells with a thickness of 3 nm for two different buffer layers

reducing the recombination rate at the *i*/*p* interface and enhance the value of V_{bi} which leads to an increment of the V_{OC}. The presence of *p*-*nc*-SiO$_x$:H window/*p*-*nc*-SiO$_x$:H buffer dual layers allowed more light to be absorbed by the absorber layer and the spectral response of the solar cell has improved in the wavelength range from 0.48 to 0.7 μm which enhance the generation rate, and an increase of J_{SC} was obtained. The improvement of J_{SC}, V_{OC} and FF leads automatically to an increase in the conversion efficiency from 7.03 % for the cell with *i*-*a*-SiC:H buffer layer to 9.67 % for the cell with *p*-*n*-SiO$_x$:H buffer layer.

ACKNOWLEDGEMENTS

The authors are grateful to Professor S. Fonash from the Pennsylvania State University for providing the AMPS-1D program used in this study.

REFERENCES

1. Jin Wang, Ke Tao, Hongkun Cai, Dexian Zhang, Guofeng Li, *Mater. Sci. Semicond. Proc.* **25**, 186 (2014).
2. A. Belfar, H. Ait-Kaci, *Thin Solid Films* **525**, 167 (2012).
3. T. Aernouts, P. Vanlaeke, W. Geens, J. Poortmans, P. Heremans, S. Borghs, R. Mertens, R. Andriessen, L. Leenders, *Thin Solid Films* **451-452**, 22 (2004).
4. T. Soderstrom, F.-J. Haug, V. Terrazzoni-Daudrix, C. Ballif, *J. Appl. Phys.* **103**, 114509 (2008).
5. B. Rech, C. Beneking, H. Wagner, *Sol. Energ. Mater. Sol. C.* **41-42**, 475 (1996).
6. S. Ogawa, M. Okabe, T. Itdh, N. Yoshida, S. Nonmura, *Thin Solid Films* **516**, 758 (2008).
7. R. Biron, C. Pahud, F.J. Haug, C. Ballif, *J. Non-Cryst. Solids* **358**, 1958 (2012).
8. J. Fang, B.J. Yan, T.T. Li, C.C. We, D.K. Zhang, B.Z. Li, Q. Huang, X.L. Chen, G.F. Hou, G.C. Wang, Y. Zhao, X.D. Zhang, *Sol. Energ. Mater. Sol. C.* **171**, 222 (2017).
9. S. Fonash, J. Arch., J. Hou, W. Howland, P. Mcelheny, A. Moquin, M. Rogosky, T. Tran, H. Zhu, F. Rubinelli, *A Manual for AMPS-1D for windows 95/NT a One-Dimensional Device Simulation Program for the Analysis of Microelectronic and Photonic Structures.* (The Pennsylvania State University: 1997).
10. A. Belfar, B. Amiri, H. Ait Kaci, *J. Nano- Electron. Phys.* **7** No 2, 02007 (2015).
11. A. Belfar, *Optik* **126**, 5688 (2015).
12. Abbas Belfar, Mohammed Belmekki, Ferroudja Hammour, Hocine Ait-Kaci, *J. Nano- Electron. Phys.* **11** No 2, 02025 (2019).
13. Baojie Yan, Guozhen Yue, Xixiang Xu, Jeffrey Yang, Sub-hendu Guha, *phys. status solidi a* **207** No 3, 671 (2010).
14. Shiyong Liu, Xiangbo Zeng, Wenbo Peng, Haibo Xiao, Wenjie Yao, Xiaobing Xie, Chao Wang, Zhangu Wang, *J. Non-Cryst. Solids* **357**, 121 (2011).
15. H. Sakai, T. Yoshida, S. Fujikake, T. Hama, Y. Ichikawa, *J. Appl. Phys.* **67**, 3494 (1990).
16. R.E. Rocheleau, S.S. Hegedus, W.A. Buchanan, S.C. Jackson, *Appl. Phys. Lett.* **51**, 133 (1987).
17. R.R. Arya, A. Catalano, R.S. Oswald, *Appl. Phys. Lett.* **49**, 1089 (1986).
18. N. Ren, J. Zhu, P. Shi, Q. Shan, T. Li, C. Wei, Y. Zhao, X. Zhang, *Sol. Energ.* **171**, 907 (2018).
19. C.T. Li, F. Hsieh, L. Wang, *Sol. Energ.* **88**, 104 (2013).

Підвищення продуктивності сонячних елементів *a*-Si:H шляхом введення наноструктурованого буферного шару *p-nc*-SiO*x*:H

A. Belfar[1], A.J. Garcia-Loureiro[2]

[1] *Laboratory of Plasma Physics, Conductor Materials and their Applications, Faculty of Physics, Oran University of Sciences and Technology Mohamed Boudiaf USTO-MB, BP1505 Oran, Algeria*
[2] *Centro de Investigación en Tecnoloxías da Información (CITIUS), University of Santiago de Compostela, Santiago de Compostela, Spain*

У роботі вивчено сонячні елементи *n-i-p* на основі гідрогенізованого аморфного кремнію (*a*-Si:H) за допомогою одновимірного коду AMPS-1D (Аналіз мікроелектронних та фотонних структур). Проаналізовано ефект введення *p*-шару на основі гідрогенізованого нанокристалічного оксиду кремнію (*p-nc*-SiO_x:H) у якості буферного шару на інтерфейсі *i*/*p* замість *i*-шару на основі гідрогенізованого аморфного карбіду кремнію (*i-a*-SiC:H). Встановлено, що включення буферного шару *p-nc*-SiO_x:H на інтерфейсі *i*/*p* зменшує смугу невідповідності між шаром поглинача *i-a*-Si:H та шаром вікна p^+-*nc*-SiO_x:H і мінімізує густину дефектів поблизу інтерфейсу. Отримано також, що спектральний відгук сонячного елементу покращився в діапазоні довжин хвиль від 0,48 до 0,7 мкм при використанні подвійних буферних *p*-шарів *p-nc*-SiO_x:H window/*p-nc*-SiO_x:H. Отже, отримано покращену продуктивність вихідних сонячних елементів із буферним шаром *p-nc*-SiO_x:H. У цьому випадку струм короткого замикання (J_{sc}) збільшується з 10,18 мА/см^2 з буферним шаром *i-a*-SiC:H до 13,44 мА/см^2 з буферним шаром *p-nc*-SiO_x:H, напруга холостого ходу (V_{OC}) покращується від 930 мВ до 941 мВ, а коефіцієнт заповнення (FF) збільшується з 74,2 % до 76,5 %. Як наслідок, коефіцієнт корисної дії зростає з 7,03 % до 9,67 %.

Ключові слова: Сонячний елемент, *a*-Si:H, *p-nc*-SiO_x:H, *i-a*-SiC:H, Буферний шар, Моделювання, Спектральний відгук.